Biomimetic tri-layered small-diameter vascular grafts with decellularized extracellular matrix promoting vascular regeneration and inhibiting thrombosis with the salidroside ☆

Jie Shi [a,b,c], Yanjiao Teng [a,b,c], Duo Li [a,b,c], Ju He [d], Adam C. Midgley [e], Xiaoqin Guo [a,b,c], Xiudan Wang [a,b,c], Xinran Yang [a,b,c], Shufang Wang [e], Yakai Feng [f,g,h], Qi Lv [a,b,c,**], Shike Hou [a,b,c,*]

[a] *Wenzhou Safety (Emergency) Institute of Tianjin University, Wenzhou, 325026, China*
[b] *Institute of Disaster and Emergency Medicine, Tianjin University, Tianjin, 300072, China*
[c] *Key Laboratory for Disaster Medicine Technology, Tianjin, 300072, China*
[d] *Vascular Surgery, Tianjin First Central Hospital, Tianjin, 300192, China*
[e] *Key Laboratory of Bioactive Materials for the Ministry of Education, College of Life Sciences, Nankai University, Tianjin, 300071, China*
[f] *School of Chemical Engineering and Technology, Tianjin University, Tianjin, 300072, China*
[g] *Frontiers Science Center for Synthetic Biology, Tianjin University, 30072, China*
[h] *Key Laboratory of Systems Bioengineering (MOE), Tianjin University, 30072, China*

ARTICLE INFO

ABSTRACT

Small-diameter vascular grafts (SDVGs) are urgently required for clinical applications. Constructing vascular grafts mimicking the defining features of native arteries is a promising strategy. Here, we constructed a tri-layered vascular graft with a native artery decellularized extracellular matrix (dECM) mimicking the component of arteries. The porcine thoracic aorta was decellularized and milled into dECM powders from the differential layers. The intima and media dECM powders were blended with poly (L-lactide-co-caprolactone) (PLCL) as the inner and middle layers of electrospun vascular grafts, respectively. Pure PLCL was electrospun as a strengthening sheath for the outer layer. Salidroside was loaded into the inner layer of vascular grafts to inhibit thrombus formation. *In vitro* studies demonstrated that dECM provided a bioactive milieu for human umbilical vein endothelial cell (HUVEC) extension adhesion, proliferation, migration, and tube-forming. The *in vivo* studies showed that the addition of dECM could promote endothelialization, smooth muscle regeneration, and extracellular matrix deposition. The salidroside could inhibit thrombosis. Our study mimicked the component of the native artery and combined it with the advantages of synthetic polymer and dECM which provided a promising strategy for the design and construction of SDVGs.

1. Introduction

The global issue of cardiovascular disease (CVD) is expounded by its associated high mortality rates [1]. Vascular transplantation is an effective method employed for the clinical treatment of CVD, and autologous vessels are widely considered the gold standard for vascular transplantation procedures [2]. However, autologous vessels have several limitations, such as mismatched size and pre-existing pathologies dependent on the patient's condition, among other reasons for transplant restrictions [3,4]. Thus, there is an increased clinical demand for artificial vascular grafts. Large-diameter artificial vascular grafts have been successfully used in clinical settings [5]. However, small-diameter vascular grafts (SDVGs, $\varphi \leq 6$ mm) are prone to failure due to the high incidence of acute thrombosis, intimal hyperplasia, and calcification [6–8]. Therefore, there is an urgent need to develop SDVGs that combine engineered capacity with compatible biomechanics and histocompatibility to guarantee long-term patency.

Constructing grafts mimicking the defining features of native tissues

---

is a promising strategy for regenerative medicine [9–12]. The native blood vessel arterial wall is composed of three different layers: the intima; media; and adventitia [13]. The intima is the innermost of the three concentric layers and consists of a continuous monolayer of endothelial cells (ECs) on a basement membrane and a thin subendothelial extracellular matrix (ECM). The media is the middle layer, comprising smooth muscle cells (SMCs) with aligned fibrous ECM enriched with bundles of elastin fibers. The adventitia consists of a collagenous ECM populated by fibroblasts and perivascular nerve cells [14]. Currently, neither natural nor synthetic materials have adequately simulated the complicated cellular microenvironment of blood vessels [15]. Incorporating components of the native ECM into a synthetic graft has been suggested to provide a biomimetic microenvironment more closely resembling native tissue that is also conducive to promoting tissue regeneration [16–18]. The native ECM of blood vessels is a complex mixture of various types of collagen proteins, polysaccharides, and bioactive factors [15]. Through physical or chemical methods, cellular components can be removed from vessel tissue. Collagen, elastin, and entrapped growth factors can be preserved as dECM. The dECM is a promising basal material, which has been employed in the preparation of scaffolds for the repair of various tissue types [19], such as skeletal muscle [20] and cartilage [15]. Reid and colleagues selected the bovine aorta and myocardium, decellularized the tissues, and milled the ECM into powder before preparing fibrous sheets to facilitate enhanced human umbilical vein endothelial cell (HUVEC) adherence and proliferation [16]. This process exemplified the reprocessing of appropriate dECM powder into structures that mimic the native environment. In the context of vascular grafts, electrospinning is a frequently utilized technique that can be employed to generate multi-layered microfiber scaffolds that exhibit close mimicry of the natural artery's differential layer structure [21].

The long-term performance of SDVGs is significantly impacted by thrombosis and occlusion, leading to graft failure [22,23]. The exposure of the ECM, of which the major adhesive proteins are fibrinogen, von Willebrand factor (vWF), and the fibrillar collagen types I and III. Platelets can bind directly to fibrinogen and vWF already present in the ECM. The collagens are not only important adhesive proteins but also potent platelet agonists leading to platelet aggregation [24]. Salidroside is an active ingredient extracted from the medicinal plant, *Rhodiola rosea*, and has reported inhibitory actions on platelet function and thrombosis through regulation of AKT/GSK3β signaling [25]. In addition, salidroside was shown to promote neovascularization [26], have pro-angiogenic [27], anti-apoptotic [28], anti-inflammatory [29], and antioxidant properties [30]. Therefore, salidroside has potential advantages as an anticoagulant for vascular graft applications without exhibiting the disadvantages commonly associated with heparin, such as the adverse effects of driving osteoporosis, thrombocytopenia, and hypersensitivity [31].

In this study, we developed tri-layered biomimetic SDVGs that combined electrospun PLCL polymer microfibers with dECM powders derived from the differential layers of porcine thoracic aortae. PLCL, with its excellent mechanical properties and compliance matching with natural blood vessels, has already been approved by the FDA for clinical applications [30,32]. The inner layer incorporated the salidroside to elicit antithrombotic effects, whereas the outer layer consisted of thicker electrospun PLCL microfibers to form a structural sheath. The physico-chemical properties, hemocompatibility, cytocompatibility, and influence on the HUVEC behavior of the scaffold were evaluated. The endothelialization, smooth muscle layer regeneration, ECM deposition, and degradability of the SDVGs were evaluated following the implant in rat abdominal aorta replacement models for 3 and 6 weeks. The results of this study provide a promising strategic approach to the design and engineering of SDVGs that more closely resemble native vascular tissue ECM microenvironments.

2. Methods

2.1. Materials

PLCL pellets (50:50; viscosity: 2.6–2.8) were purchased from Jinan Daigang Biomaterials (Jinan, China). Salidroside and 1, 1, 1, 3, 3, 3-hexafluoro-2-propanol (HFIP) were purchased from Shanghai Macklin Biochemicals (Shanghai, China). Sprague-Dawley (SD) rats were purchased from Beijing HFK Biotechnology (Beijing, China). Porcine thoracic aortae were obtained from Tianjin Yingbin Meats (Tianjin, China).

2.2. Decellularized extracellular matrix powder production

The detailed information of the decellularization procedure is provided in the supporting information. After decellularization, we peeled off the intima, media, and adventitia separately by standard anatomical instruments and freeze-dried. The decellularization effect was evaluated by genomic DNA detection, Hematoxylin & Eosin (H&E) staining, Masson's trichrome staining, Verhoeff-Van Gieson (VVG) staining, and Alcian Blue staining. To observe the morphological characterization of samples, which were mounted on aluminum foil and sputter-coated with gold. Scanning electron microscopy (SEM) (Apreo S LoVac, Czech FEI) at an accelerating voltage of 15 kV.

The intima and media samples were then milled into powder using a liquid nitrogen grinder (SPEX SamplePrep, Freezer Mill, USA). The size distribution of dECM powder was detected using a nanoparticle size and zeta potential analyzer (Litesizer 500, Austria Anton Paar).

2.3. Scaffold preparation

Scaffolds corresponding to three individual layers of the vascular grafts were prepared by electrospinning. The preparation process for the inner layer electrospinning solution was as follows: PLCL solution (10%, w/v) and salidroside (Sal) were dissolved in HFIP. Then, the intima dECM powder (1%, w/v) was added to the solution and stirred. The preparation process for the middle layer electrospinning solution was as follows: PLCL solution (10%, w/v) was dissolved in HFIP before media dECM powder (1%, w/v) was added. The outer layer electrospinning solution comprised PLCL (10%, w/v) dissolved in HFIP. The tri-layer electrospun vascular grafts (PLCL-dECM-Sal) were prepared by sequential three-step electrospinning. Firstly, the inner layer was electrospun for 10 min, then the middle layer for 10 min, and then the outer layer for a further 5 min. The flow rates of the inner, middle, and outer layers were 2 mL/h, 4 mL/h, and 4 mL/h, respectively. A stainless-steel rod collector (2 mm in diameter) was used to prepare the vascular grafts. Membranes were prepared with the same condition and using a grounded metal mandrel (10 cm in diameter). The obtained membranes and vascular grafts were vacuum-dried for 48 h to remove the residual solvents. The pure PLCL and PLCL-dECM vascular grafts were used as the control group.

2.4. Characterization of scaffolds

SEM was used to observe graft and membrane morphologies. The average fiber diameter was measured and calculated using ImageJ software (NIH) ($n = 5$). The HUVEC and SMC proliferation on different layers of scaffolds was evaluated by CCK8 assay (Sparkjade Biotechnology Co., Ltd., Shandong). The mechanical properties of vascular graft were assessed by a tensile testing machine (Intron) with a load capacity of 1 KN. The stress-strain curves of grafts were recorded and the Young's moduli were calculated based on the slope of the stress-strain curve in the elastic region. For burst pressure, according to a previous report [33]. In brief, burst pressure was measured by filling a graft of 3 cm in length with

soft paraffin (Vaseline), clamping one end and hermetically sealing the other end to a vascular catheter. After the sample was incubated at 37 °C for 30 min, the Vaseline was filled at a rate of 0.1 mL/min. The filling pressure was recorded until the graft wall burst ($n = 5$). The water contact angle (WCA) of membrane scaffolds was measured using an optical contact goniometer (Harke-SPCA, China) ($n = 5$). Scaffolds were cut into 5 mm^2 segments for the fourier transform infrared spectroscopy (FTIR) test. All spectra were obtained using a Nicolet iS10 spectrometer with a Smart iTX diamond attenuated total reflection detector (Thermo Fisher Scientific). Spectra were acquired between 4000 and 400 cm^{-1} with a resolution of 1 cm^{-1} using OMNIC Spectra software (Thermo Fisher Scientific) ($n = 3$).

2.5. In vitro release of salidroside

In vitro release of salidroside from tri-layer electrospun grafts was quantified using high-performance liquid chromatography (HPLC). The grafts (20 mg) were soaked in 1 mL phosphate-buffered saline (PBS) buffer. Samples ($n = 3$) were then incubated at 37 °C. At the time of 2, 6, 12, 24, 36, 48, 72, and 96 h, supernatants were collected and stored at -20 °C for analysis, with 1 mL fresh PBS used to replenish the starting volume. The salidroside in the supernatant was measured using the LCMS-20AD system (Shimadzu, Kyoto, Japan). The salidroside was measured over 10 min using an excitation wavelength of 275 nm.

2.6. In vitro hemocompatibility evaluation

2.6.1. Haemolysis assay

The haemolysis assay was performed according to the reported literature [34]. Briefly, blood was obtained from rats and diluted. The samples (1 cm in diameter) were placed in 0.9% NaCl solution at 37 °C for 30 min. Then the diluted blood was added to samples and incubated at 37 °C for another 60 min. Saline or distilled water was used as the negative and positive control groups, respectively. Subsequently, the samples were centrifuged for 5 min at 3000 rpm, and the absorbance of the supernatant was recorded at 545 nm with a full wavelength microplate reader (Epoch, BioTek, US). The haemolysis percentage was calculated according to the following equation: Haemolysis (%) = $(A_1-A_2)/(A_3-A_2) \times 100\%$, where A_1, A_2, and A_3 are the absorbances of the sample, negative control, and positive control, respectively. The data were averaged from measurements on five samples.

2.6.2. Platelet adhesion

To test platelet adhesion, sample membranes (1 cm in diameter) were placed in 48-well cell culture plates ($n = 5$). To each well, 300 μL rat platelet enriched plasma (PRP) was added, and the samples were incubated at 37 °C for 2 h. The unattached platelets were removed by rinsing 3 times with PBS. Then fixed with 2.5% glutaraldehyde and dehydrated with gradient ethanol, observed by SEM.

2.7. The effect of scaffold on HUVEC behavior

2.7.1. HUVEC adhesion

The membrane scaffolds were placed in 48-well cell culture plates. HUVECs (3×10^4/well, $n = 3$) were seeded on the membrane scaffolds. Then the plates were placed in an incubator for 24 h. The medium was removed and scaffolds were fixed with 2.5% glutaraldehyde overnight, subsequently dehydrated by graded ethanol and observed by SEM.

2.7.2. HUVEC migration assay

Preparation extraction of scaffolds: membrane scaffolds were added to the cell culture medium at a density of 6 cm^2/mL, immersed at 37 °C for 24 h, and then the extraction was collected for the following experiments. HUVECs were seeded in 24-well cell culture plates. When cells reached 80–90% confluence, scratch wounds were made with 200 μL

sterile pipette tips. The detached cells were removed by washing with PBS, and the extractions from different scaffolds were added to plates ($n = 3$). Immediately, images were taken under an inverted microscope (Nikon Eclipse Ti–U, Tokyo, Japan). After 12 h of incubation, the cells that had migrated into the scratched area were photographed at the same position and using the same inverted microscope. The migration rate was calculated using Image J software (NIH) and reported as the percentage of wound healing, which was calculated according to the following equation: Wound healing rate (%) = (wound width at 0 h - wound width at 12 h)/wound width at 0 h × 100% [35].

2.7.3. HUVEC tube formation assay for in vitro angiogenesis

Tube formation assays were performed according to previously reported procedures [36]. In brief, 50 μL of cold Matrigel (Corning, Tewksbury, MA, USA) was added to a 48-well cell culture plate and incubated at 37 °C. After gelation, HUVECs were seeded onto Matrigel-coated wells (1×10^5 cells/well) and cultured with extractions prepared from the different scaffolds. Four hours later, tube formation was observed under an inverted microscope, and images ($n = 3$) were captured from each well. The total tubes formed by HUVECs in each image were counted using Image J software (NIH).

2.8. Abdominal aorta replacement of rat

Animal experiments were approved by the Animal Experiment Ethics Committee of the Institute of Radiation Medicine, the Chinese Academy of Medical Sciences (IRM-DWLL-2020015) and complied with the National Institutes of Health Guideline for Care and Use of Laboratory Animals. Rat abdominal aorta replacement models were used to assess the performance of the vascular grafts *in situ*. The procedure was carried out as described previously [37]. Briefly, SD rats (male, weight 300–320 g) were randomly assigned into three groups (PLCL, PLCL-dECM, PLCL-dECM-Sal) and divided among two-time points (3 and 6 weeks, $n = 4$). Heparin (100 units/kg) was injected through tail veins for anticoagulation before surgery. A middle laparotomy incision was performed, and the unbranched abdominal aorta was isolated, clamped, and transected. The tubular grafts (2.0 mm in inner diameter, 350 μm in thickness, and 1.2 cm in length) were sewn in an end-to-end fashion using 9-0 monofilament nylon sutures. No anticoagulation drugs were administered after surgery. Rats were sacrificed at week 3 and 6, and grafts were explanted for analysis. Whole blood was taken for the following serum biochemical parameters test. Serum samples were analyzed by the automatic biochemical analyzer (Modular P800, Roche, USA) for levels of aspartate transaminase (AST), alanine transaminase (ALT), creatinine (CREA), total bilirubin (TBIL) to examine liver and kidney function ($n = 4$). The extent of damage to the heart and liver was measured by H&E staining.

2.9. Immunofluorescence staining

The immunofluorescence staining methods were performed as previously described [21]. Sections were stained with primary antibodies. To determine the composition of major ECM components, sections were also stained with mouse anti-collagen I (1:100), anti-collagen III (1:100), and anti-elastin antibodies (1:300). The SMCs were stained with mouse anti-α smooth muscle actin (α-SMA) antibody (1:100). Endothelial cells were stained with mouse anti-CD31 primary antibody (1:100). Secondary antibodies including Alexa Fluor 594 goat anti-rabbit IgG (H + L) (1:200), AlexaFluor-488 goat anti-mouse IgG (H + L) (1:200) and AlexaFluor-488 goat anti-rabbit IgG (1:200). Nuclei were counterstained with DAPI-containing mounting solution (Fluoromount G, Southern Biotech, USA). The immunofluorescence stained sections were imaged using a fluorescence microscope with mounted camera (Nikon, Eclipse Ni, Japan). The endothelial coverage rate and the average thickness of SMCs were calculated using ImageJ software (NIH).

2.10. Histological analysis

The explants were sectioned to 5 μm in thickness after being embedded in OCT. Subsequently, the cross-sections of explanted grafts were stained with H&E to evaluate cell infiltration. Safranin O staining to observe glycosaminoglycans (GAGs), Verhoeff Van Gieson (VVG) staining to observe the elastin, and Von Kossa staining to evaluate calcification. The image was viewed and captured using light microscopy (Nikon, Eclipse Ni, Japan).

2.11. Degradation test

The *in vitro* degradation behaviors of scaffold: the pre-weighed scaffolds were immersed in PBS (pH = 7.4) at 37 °C. At pre-set time points (1, 2, 4, 8, 12 weeks), the immersed scaffolds were collected, washed with deionized water three times, and then vacuum dried. The weight loss of the sample at a certain time point time was calculated according to the following equation: $W_{loss} = (W_0 - W_t)/W_0 * 100\%$. ($W_0$: an initial weight of the sample; W_t: the residual weight of the immersed sample at the conditioned time points). The morphology of scaffolds was observed by SEM.

In vivo, degradation was analyzed by observing the morphology change of explanted vascular grafts. The vascular grafts were decellularized with 0.5% SDS solution for 24 h, and then digested with 0.1% type I collagenase for 1 h. Samples were vacuum dried for SEM analysis.

2.12. Statistical analysis

The results were given in mean ± standard deviation. Statistical significance was assessed by Student's t-test (single comparisons) or one-way ANOVA (multiple comparisons). Within the figures, the significance is denoted by the following annotated markings: * for $p < 0.05$; ** for $p < 0.01$; and *** for $p < 0.001$.

3. Results

3.1. Decellularization process and effect evaluation

The decellularization of the aorta tissue is shown in Fig. 1A. The porcine thoracic aorta was decellularized using a combination of high and low permeability solution, enzyme, and detergent. The thickness of the porcine thoracic aorta wall decreased significantly and the structure became loose after decellularization (Fig. 1B). The method used was determined to be effective in achieving decellularized tissues based upon
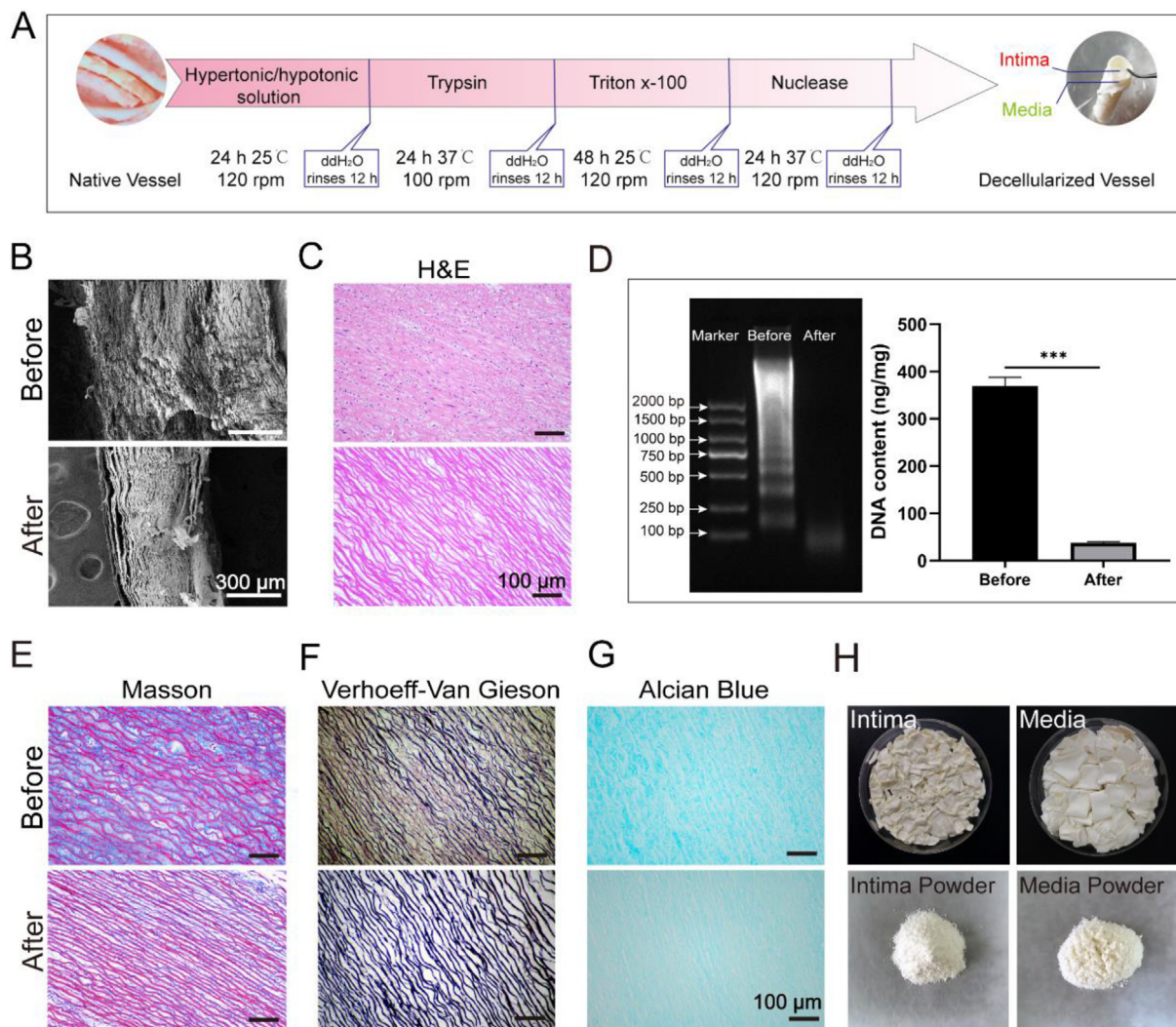

Fig. 1. Decellularization process and effect evaluation. (A) Schematic of the decellularization process. (B) The morphology before and after decellularization was observed by SEM. (C) H&E staining. (D) Genomic DNA content determination ($n = 3$, ***P < 0.001). (E) Masson's Trichrome staining. (F) Verhoeff-Van Gieson staining. (G) Alcian Blue staining. (H) The intima and media were peeled apart and freeze-dried, milled powder.

the established criteria as described previously [38,39], specifically (i) no nuclei observed by analysis of H&E staining (Fig. 1C); (ii) no DNA ≥200 base pairs observed by agarose gel analysis, and (iii) samples had a content of <50 ng dsDNA per mg initial dry weight as measured with Nanodrop (Fig. 1D). Furthermore, Masson trichrome staining showed that most of the collagenous composition was maintained after decellularization (Fig. 1E). Verhoeff-Van Gieson (VVG) staining revealed that elastic fibers were well preserved after the decellularization (Fig. 1F). Alcian blue staining showed that the content of proteoglycan decreased after decellularization (Fig. 1G). The intima and media were from porcine thoracic aorta and freeze-dried, then milled into dECM powder (Fig. 1H). The diameter distribution of 90% dECM powders was below 5 µm (Figure S1).

3.2. Characterization of scaffolds

3.2.1. Tri-layer scaffold characterization

Tri-layer vascular grafts were prepared as shown in Fig. 2A. There were three layers in PLCL-dECM and PLCL-dECM-Sal groups as defined with the white dashed line. The salidroside was loaded into the inner layer of PLCL-dECM-Sal vascular grafts (Fig. 2A). SEM images of cross-sections of grafts showed that they had favorable tubular structures (Figure S2). All vascular grafts had good elasticity which could be bent, were compressible, and could be stretched without loss of structural integrity (Fig. 2B). The lumen surface of the PLCL-dECM-Sal vascular graft SEM results showed that all fibers had a smooth surface with well-defined fiber morphology (Fig. 2C–E). The fiber diameter of the inner layer (Fig. 2F), middle layer (Fig. 2G), and outer layer (Fig. 2H) were 1.15 ± 0.15 µm, 1.37 ± 0.12 µm, and 2.84 ± 0.08 µm respectively.

HUVECs seeded on the inner layer grew better than those on the outer and middle layers (Fig. 2I). A similar trend was observed in SMCs that seeded on the middle layer, compared with the cells on the inner layer on days 1 and 3 (Fig. 2J). These results indicated that the incorporation of dECM powder from artery intima and media was more favorable to supporting the growth of HUVECs and SMCs, respectively.

3.2.2. Mechanical properties

The mechanical properties of vascular grafts were characterized by tensile stress under wet conditions. The maximum stress at break was 9.05 ± 1.54 MPa for the PLCL group, 3.51 ± 0.61 MPa for the PLCL-dECM group, and 4.46 ± 0.77 MPa for the PLCL-dECM-Sal group (Fig. 3A). The maximum elongation at break for all groups exceeded 300% (Fig. 3B). There was an identical trend observed in the elastic moduli among different groups. In detail, the elastic modulus was 3.35 ± 0.66 MPa for the PLCL group, 2.97 ± 0.62 MPa for the PLCL-dECM, and 2.93 ± 0.49 MPa for the PLCL-dECM-Sal group (Fig. 3C). The stress-strain curves of the scaffolds are shown in Fig. 3D. All kinds of vascular grafts met the mechanical requirements of vascular graft implantation (i.e., elastic modulus: 2–20 MPa, ultimate tensile stress >2 MPa, and fracture strain >60%) [21,40,41]. The burst pressure was 1811 ± 287 mmHg for the PLCL group, 1411 ± 267 mmHg for the PLCL-dECM group, and 1180 ± 191 mmHg for the PLCL-dECM-Sal group (Figure S3). The burst pressure of each graft reached the level of a native artery [42].

3.2.3. Hydrophilic properties

Water contact angles were measured to determine the hydrophilicity of scaffolds (Fig. 3E). The water contact angle of the PLCL groups was $104.52 \pm 8.1°$. The addition of dECM improved the hydrophilicity of the grafts, which reduced the contact angle of the PLCL-dECM group to nearly $84.51 \pm 11.1°$, and the PLCL-dECM-Sal group was $71.66 \pm 12.8°$.

3.2.4. Fourier transform infrared spectroscopy (FTIR) analysis

FTIR analysis was used to characterize whether dECM was successfully incorporated into the vascular grafts. It was shown that the characteristic protein peaks of 1650 cm^{-1} (amide I) and 1540 cm^{-1} (amide II) appeared in the PLCL-dECM group (Fig. 3F).

3.2.5. Release of salidroside

It was the most beneficial to HUVEC proliferation on the scaffold when the loaded concentration of salidroside was 200 µg/mL (Figure S4). The release of salidroside was in a sustained manner (Fig. 3G). In the initial 20 h, the percentage of cumulative release was approximately 45% of the total salidroside loaded into the grafts, and the burst release was within the first 10 h. Across the following days, the release rate was slowed and exhibited steady. This may be a result of the remaining ~55% of salidroside still entrapped within fibers of the scaffold, which would be expected to be released in tandem with fiber degradation.

3.2.6. Haemocompatibility

Platelet adhesion on various scaffolds was visualized by SEM (Fig. 3H). There were 60 ± 16, 83 ± 12, and 34 ± 13 platelets per field in the PLCL, PLCL-dECM, and PLCL-dECM-Sal groups respectively (Fig. 3I). The addition of dECM increased platelet adhesion (Fig. 3H2&H5). While the salidroside could significantly reduce the platelet adhesion (Fig. 3H3&H6). The hemolysis percentage of all groups was found to be below 5%. The hemolysis rate of the PLCL-dECM-Sal and PLCL-dECM groups was significantly lower than that of PLCL group (Fig. 3J).

3.3. The effect of scaffold on HUVEC behavior

The effect of scaffold on HUVEC behavior was performed in Fig. 4A. HUVECs exhibited a shrunken appearance on the PLCL scaffolds rather than full spreading of the membrane. While in PLCL-dECM and PLCL-dECM-Sal groups, HUVECs spread with a polygonal morphology, indicating that they had adhered fully (Fig. 4B), which would be beneficial to enhance the growth activity of endothelial cells. The migration rate of HUVECs in the PLCL PLCL-dECM, and PLCL-dECM-Sal groups were $27.39 \pm 7.5\%$, $46.5 \pm 5.3\%$, and $57.5 \pm 5.8\%$ respectively (Fig. 4C&E). According to these results, the addition of dECM significantly facilitated HUVEC migration. In the HUVEC tube formation assay (Fig. 4D &F)), more tubes were found in PLCL-dECM group (36 ± 1 per field) and PLCL-dECM-Sal group (39 ± 3 per field) compared with the PLCL group (25 ± 3 per field). The results demonstrated that scaffolds with incorporated dECM improved endothelial cell tube formation.

3.4. The performance of grafts as rat abdominal aorta substitutes

3.4.1. Patency and luminal morphology

The vascular grafts were transplanted into rat abdominal aortae for 3 and 6 weeks (Fig. 5A). All vascular grafts were kept patent in the PLCL-dECM-Sal group (Fig. 5B). The cross-section and luminal surface of PLCL-dECM-Sal vascular grafts remained smooth and clean (Fig. 5C). Surprisingly, we found that the density of capillaries within the PLCL-dECM-Sal vascular graft wall was distinctly more than that of the other two groups at week 6 (indicated by the black arrow) While in the PLCL group and the PLCL-dECM group, there was one vascular graft was seriously blocked respectively (Figure S5).

3.4.2. In vivo biocompatibility of the vascular grafts

The *in vivo* biocompatibility was evaluated by heart and liver pathological and serum indices analysis. No severe damage, histological abnormalities, or inflammatory lesions were observed in the heart and liver after vascular graft implantation (Fig. 5D). Furthermore, the vascular graft implantation did not significantly affect serum indices (ALT, AST, CREA, TBIL), the levels in each group showed no significant difference compared to the control group, revealing no apparent toxicity to the rat liver and kidney (Fig. 5E).
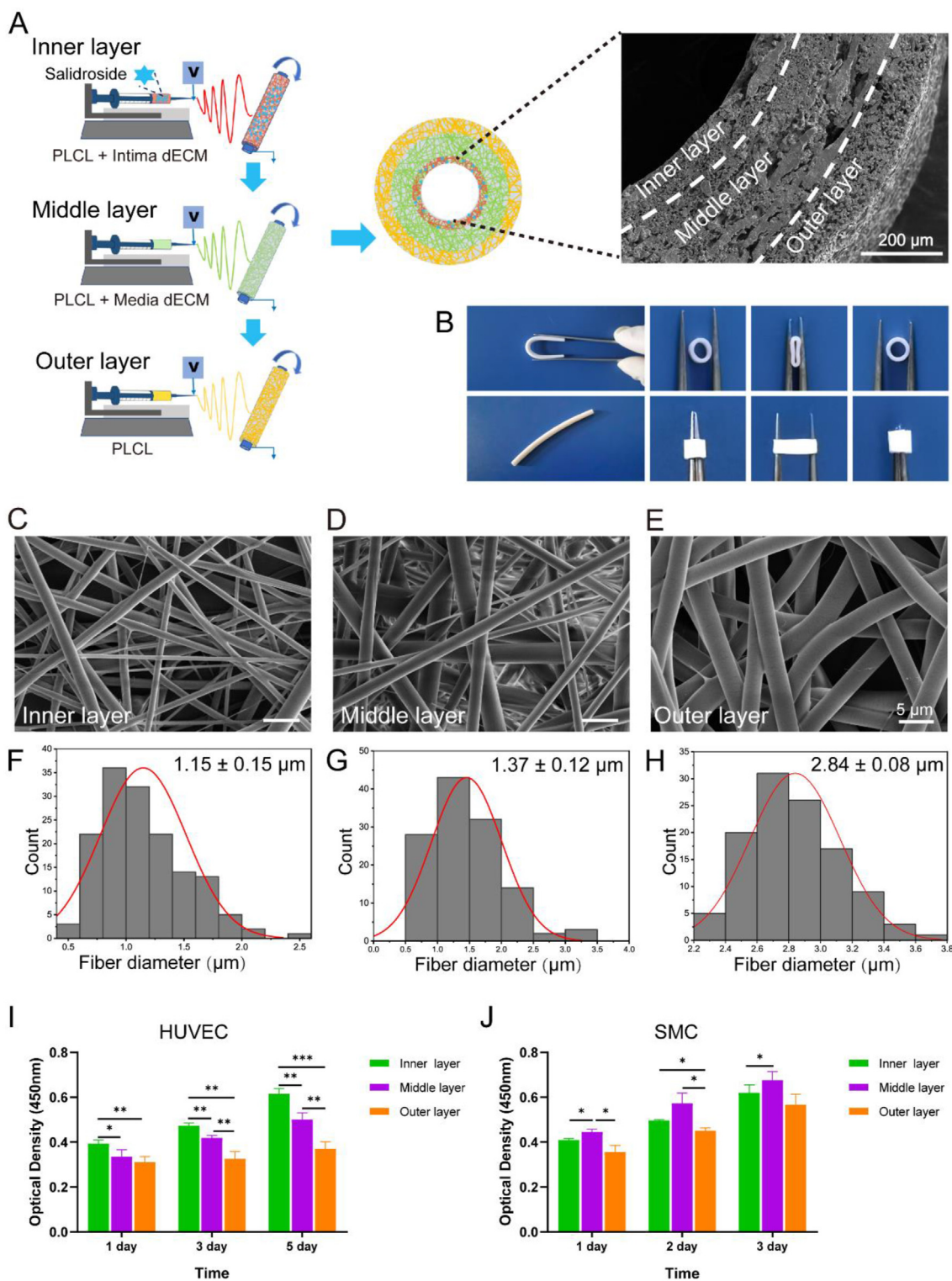
Fig. 2. Tri-layer scaffold characterization. (A) Preparation and morphology of PLCL-dECM-Sal vascular grafts. (B) Macroscopic morphology of PLCL-dECM-Sal vascular grafts. Micromorphology and fiber diameter distributions of PLCL-dECM-Sal vascular grafts: (C & F) inner layer, (D & G) middle layer, and (E & H) outer layer. The proliferation of (I) HUVECs and (J) SMCs on different layers of scaffolds ($n = 5$). (*$P < 0.05$, **$P < 0.01$, ***$P < 0.001$).

3.4.3. Endothelialization

The luminal surface of grafts was observed at three different locations by SEM: near the anastomosis site, at the midpoint, and between them (Fig. 6A–C). At week 6, cell coverage was continuous which had expanded on all grafts in PLCL-dECM and PLCL-dECM-Sal groups, whilst was scattered in PLCL grafts. Some fibers in the PLCL group were still not

occupied by cell coverage, as observed in the magnified images (Fig. 6A1-A3).

Herein, the endothelial layer formation of vascular grafts was demonstrated by immunofluorescence staining of CD31. The monolayer consisting of endothelial coverage was approximately 50% in the PLCL group (Fig. 6D&G) but 80% in PLCL-dECM and PLCL-dECM-Sal groups
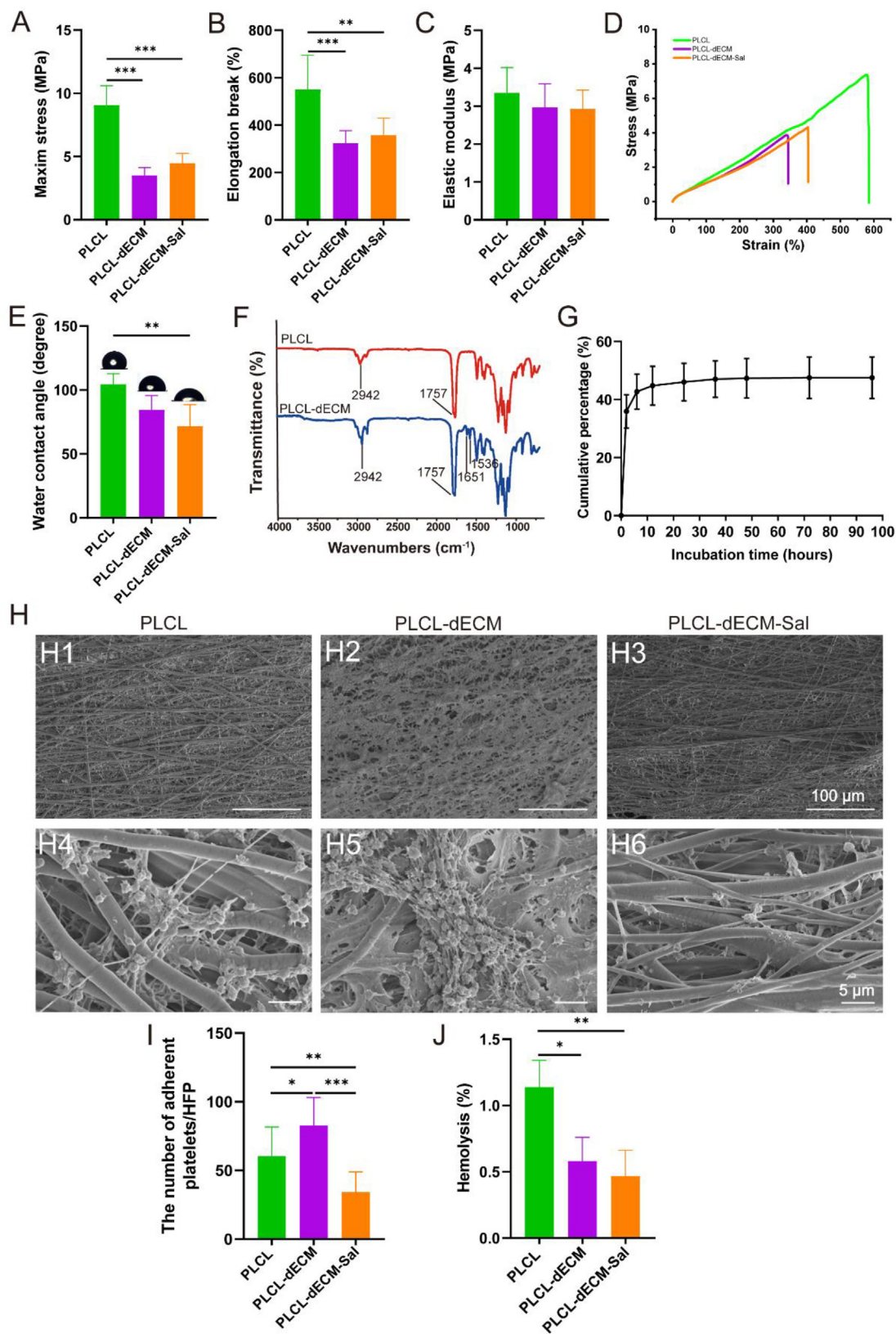
Fig. 3. Scaffold characterization. (A) Maximum stress ($n = 5$). (B) Elongation break ($n = 5$). (C) Elastic modulus ($n = 5$). (D) Representative stress-strain curves ($n = 5$). (E) Water contact angle ($n = 5$). (F) Representative FTIR analysis ($n = 3$). (G) The percentage of salidroside cumulative release from vascular grafts ($n = 3$). (H) Platelet adhesion on scaffolds observed by SEM (H4–H6 was the magnification of H1–H3). (I) Quantitative data for the adhesion of platelets based on the SEM images ($n = 5$). (J) Hemolysis rate of scaffolds ($n = 5$). (*$P < 0.05$, **$P < 0.01$, ***$P < 0.001$).
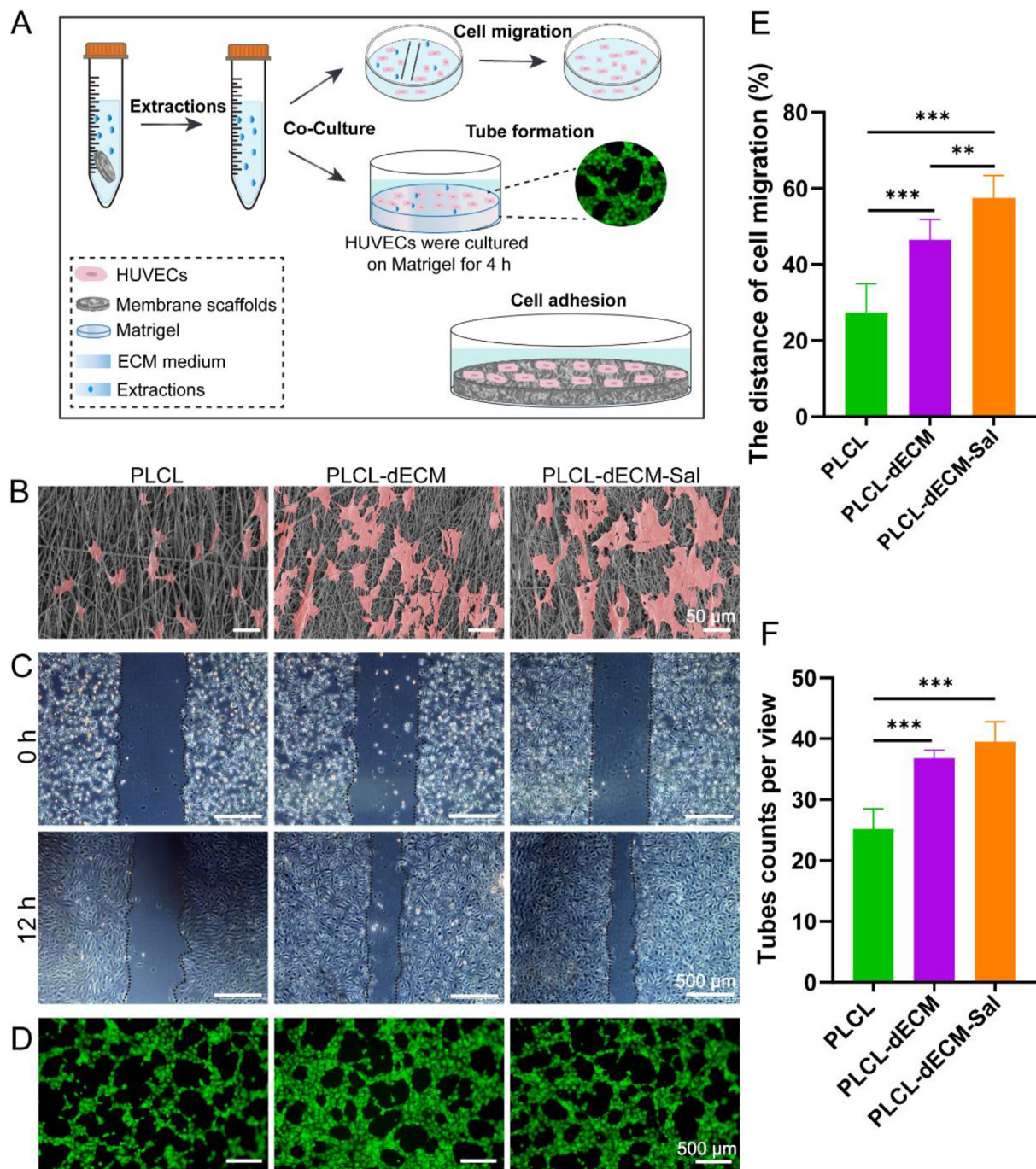
Fig. 4. The effect of scaffold on HUVEC behavior. (A) The effect of scaffold on HUVEC behavior experiment scheme. (B) The adhesion (C&E) migration and (D&F) tube formation of HUVEC on scaffolds. ($n = 3$, *P < 0.05, **P < 0.01, ***P < 0.001).

(Fig. 6E–G). These results indicated that the addition of dECM powder into the PLCL fiber scaffolds significantly promoted the endothelialization of the vascular graft.

3.5. Smooth muscle regeneration and ECM deposition

The smooth muscle regeneration was detected by immunofluorescence staining with α-SMA (Fig. 7A–D). At week 6, the average thickness of α-SMA$^+$ cell layers in both PLCL-dECM and PLCL-dECM-Sal groups was thicker than the PLCL group (Fig. 7D). These data suggested that dECM incorporation promoted smooth muscle regeneration.

ECM deposition was evaluated by histological and immunofluorescent staining at week 6. H&E staining showed that a large number of cells

infiltrated into the PLCL-dECM and PLCL-dECM-Sal graft wall and secreted substantial ECM with high density (Fig. 7E). Safranin O staining showed that the deposition of glycosaminoglycans in PLCL-dECM and PLCL-dECM-Sal grafts was much richer than that in PLCL grafts (Fig. 7F). VVG staining showed that the expression of elastin in the wall of PLCL-dECM and PLCL-dECM-Sal grafts was discontinuous and significantly increased (Fig. 7G). However, only a small amount of elastin was scattered in the wall of PLCL grafts. Von Kossa staining was used to assess the occurrence of ECM calcification in grafts. Calcification (indicated by red arrows) was founded in PLCL-dECM and PLCL-dECM-Sal groups (Fig. 7H). Notably, the extent of calcification observed in the PLCL-dECM group was more serious than in the PLCL-dECM-Sal group. In addition, the immunofluorescent staining of collagen I and III and elastin result
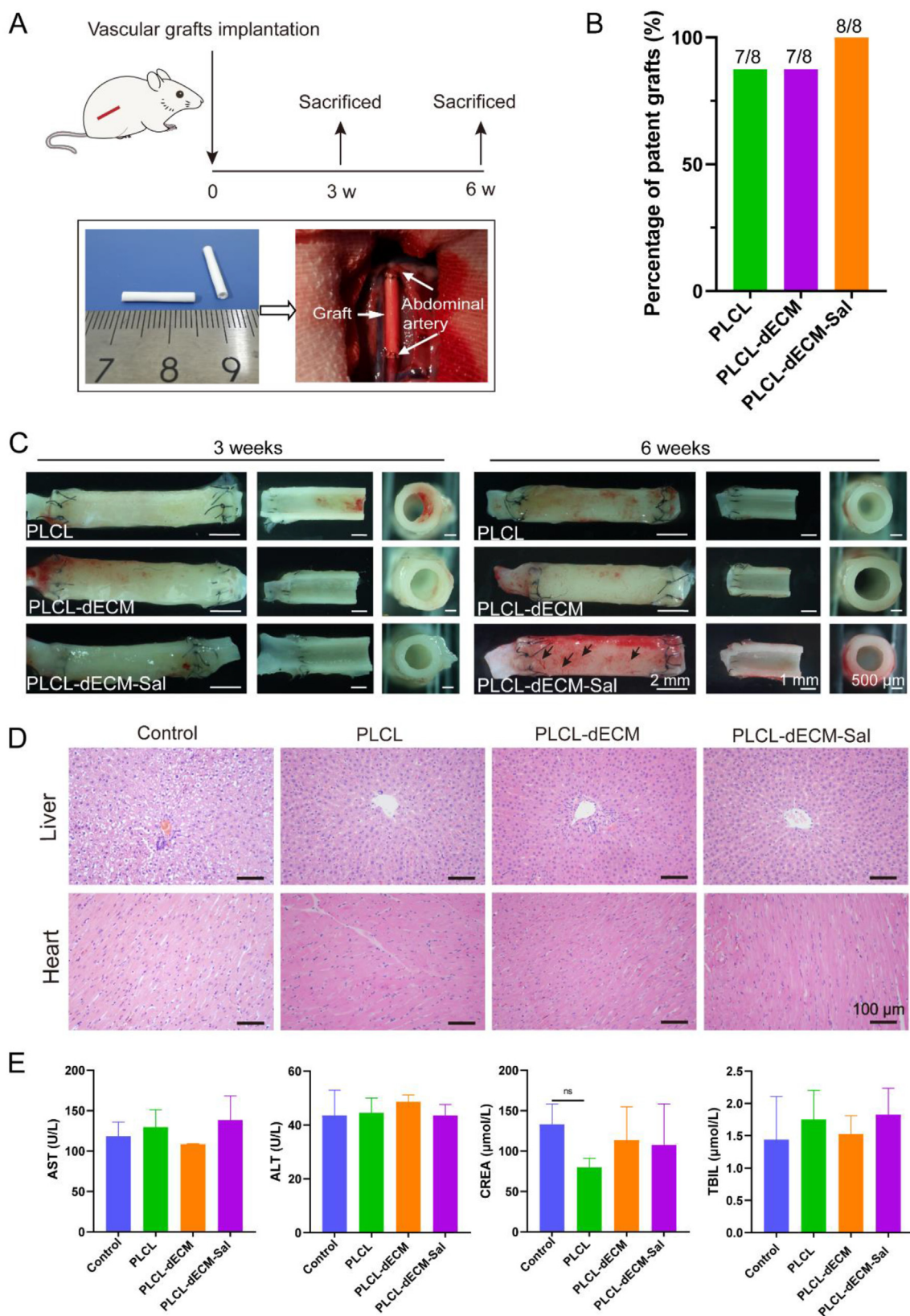
Fig. 5. The performance of the vascular grafts. (A) The vascular graft rat abdominal aorta replacement models for 3 and 6 weeks. (B) The percentage of patent vascular grafts ($n = 8$) for the sum of week 3 and week 6 in each group. (C) The luminal morphologies of grafts were observed by stereomicroscopy ($n = 4$). (D) H&E staining of rat heart and liver ($n = 4$). (E) Serum AST, ALT, CREA and TBIL levels ($n = 4$).
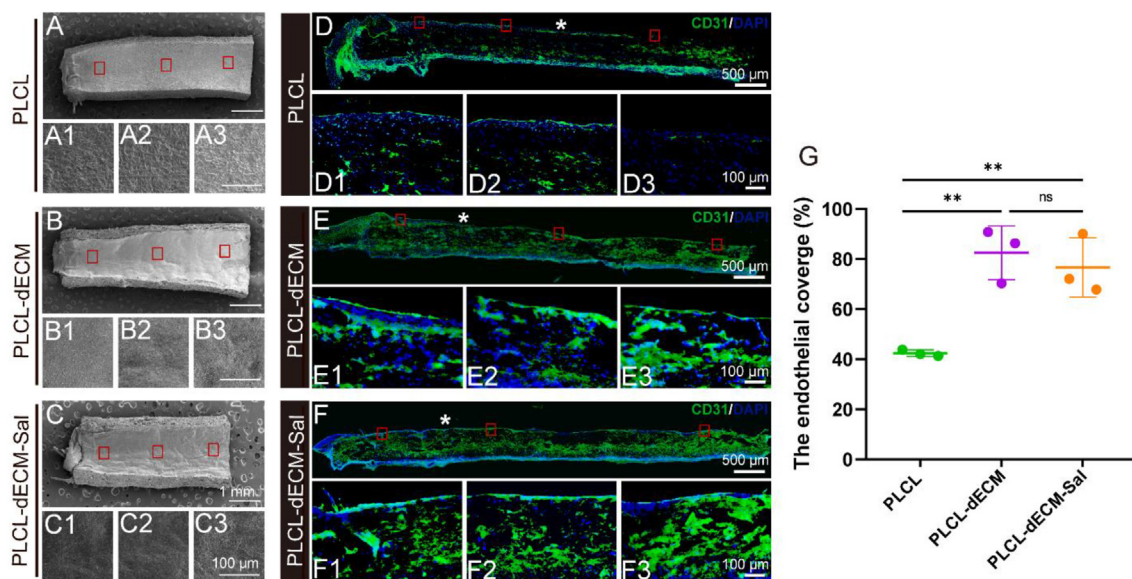
Fig. 6. Endothelialization of vascular grafts at week 6. (A-C3) Luminal surface morphologies of grafts. (D–G) The CD31 immunofluorescence staining of vascular grafts. ($n = 3$, Small images were high-magnification images of the left, middle, and right areas of the grafts as indicated by the red box; * indicated the lumen of vascular graft; **P < 0.01).
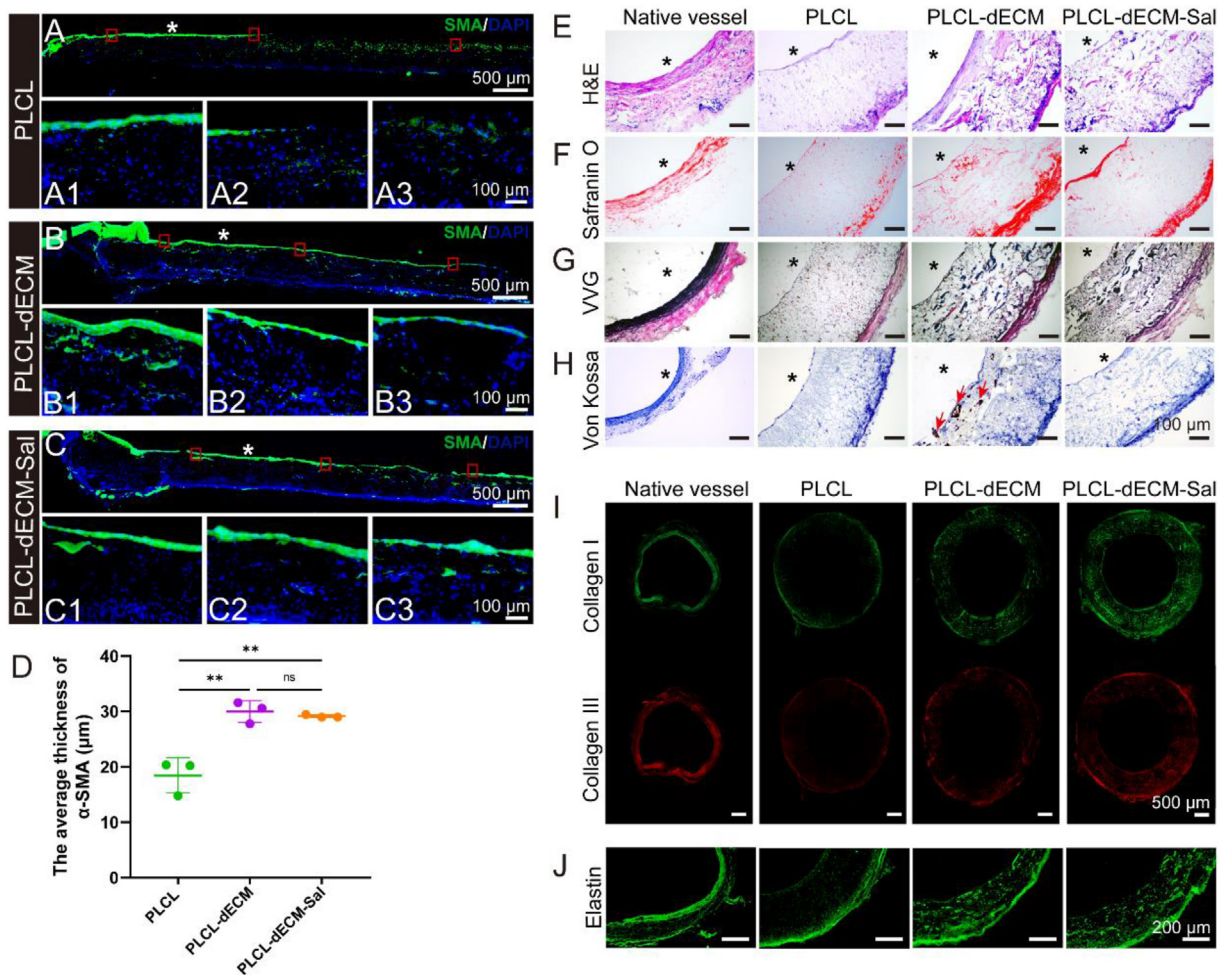

Fig. 7. Smooth muscle regeneration and ECM deposition at week 6. (A–C) The α-SMA immunofluorescence staining of vascular grafts (Small images were high-magnification images of the left, middle and right areas of the grafts as indicated by the red box). (D) Quantification of the average thickness of α-SMA⁺ layers ($n = 3$). (E) H&E staining. (F) Safranin O staining. (G) VVG staining. (H) Von kossa staining. (I) Immunofluorescent staining of collagen I and III. (J) Immunofluorescent staining elastin. (*P < 0.05, **P < 0.01, ***P < 0.001. Image annotations (*) indicate lumen position).

showed that the expression of collagen and elastin in PLCL-dECM and PLCL-dECM-Sal grafts were much richer than that of PLCL grafts (Fig. 7I–J). These results exhibited that the grafts with dECM were able to improve the deposition of ECM.

3.6. Degradability of scaffold

The degradation rate of implanted materials is a key factor dictating tissue regeneration. The degradability of scaffolds was performed *in vitro* for 12 weeks. There were more fiber fractures in PLCL-dECM and PLCL-dECM-Sal groups than in the PLCL group as shown in SEM images (indicated by the red arrows) (Fig. 8A). However, there was no significant difference in loss of mass in scaffolds of all groups (Figure S6). *In vivo*, degradation at week 3 and 6 was shown in Fig. 8B. The fiber fractures were not as apparent at week 3 compared to the evident fracture observable at week 6. The groups of PLCL-dECM and PLCL-dECM-Sal grafts, in comparison to the PLCL, exhibited extensive evidence of breakages, and the fibers had been degraded into smaller fragments by 6 weeks. Taken together, these data demonstrated that the addition of dECM accelerated the degradation rate of PLCL fibers within scaffolds.

4. Discussion

Despite extensive research devoted to the study of SDVGs, there remain prominent challenges in this research field. In this study, we developed a tri-layered biomimetic SDVGs composed of PLCL and porcine artery dECM by electrospinning loaded with salidroside. PLCL-dECM-Sal SDVGs promoted the proliferation, migration, tube formation, and adhesion of HUVECs *in vitro* and in rat abdominal aorta transplantation models, demonstrated feasibility as SDVGs for implantation, with favorable pro-regenerative outcomes lacking incidence of pathological tissue repair.

Timely endothelialization plays a crucial role in maintaining vascular homeostasis and preventing vascular disease [43]. There have been numerous strategies employed to achieve the purpose of rapid endothelialization induced by SDVGs, such as lumen functionalization with peptides [44]. Growth factors [45], nitric oxide release and passive generation [46], or the pre-seeding of scaffolds with mesenchymal stem cells [47]. In this study, we utilized a readily accessible method that incorporated powdered dECM obtained from differential aorta layers into the graft fabrication stage. By electrospinning the dECM powder with PLCL into scaffold fibers, we demonstrated the significant promotion of the endothelialization effect of PLCL-dECM SDVGs by providing a hydrophilic microenvironment conducive to endothelial cell growth, which facilitated cell adhesion and infiltration. It is well known that a slightly hydrophilic surface is more conducive to cell adhesion [48], which is one possible solution to promote cell growth on and into grafts. In turn, the infiltrated cells produce matrix metalloproteinases, which accelerate the degradation of scaffolds and facilitate ECM remodeling [49]. Our results supported the rationale for including material components sourced from native tissues to enhance the tissue regenerative effects of SDVGs.

Salidroside was loaded into the intima layer of the grafts to reduce the adhesion of platelets and inhibit the occurrence of thrombus. Although salidroside alone had no obvious effect on promoting angiogenesis, when salidroside and dECM were incorporated into the graft layers, a synergistic promotion of angiogenesis was observed. We speculate that this positive effect was explained by the influence of salidroside on the induction of endothelial cell tube formation, as observed *in vitro*.

The vascular grafts existed slightly calcification during implantation. The reasons for the calcification can be summarized in the following two points: (i) on one hand, PLCL generates acid during the degradation process and acidic environments may induce calcification [50]; (ii) on the other hand, the addition of dECM may have increased binding sites for calcium ions, facilitating the deposition of calcium during ECM remodeling [51]. A previous study suggested that salidroside inhibition of high glucose-dependent vascular SMC proliferation may be related to its antioxidant activity [52], but the study of the effects of salidroside in a
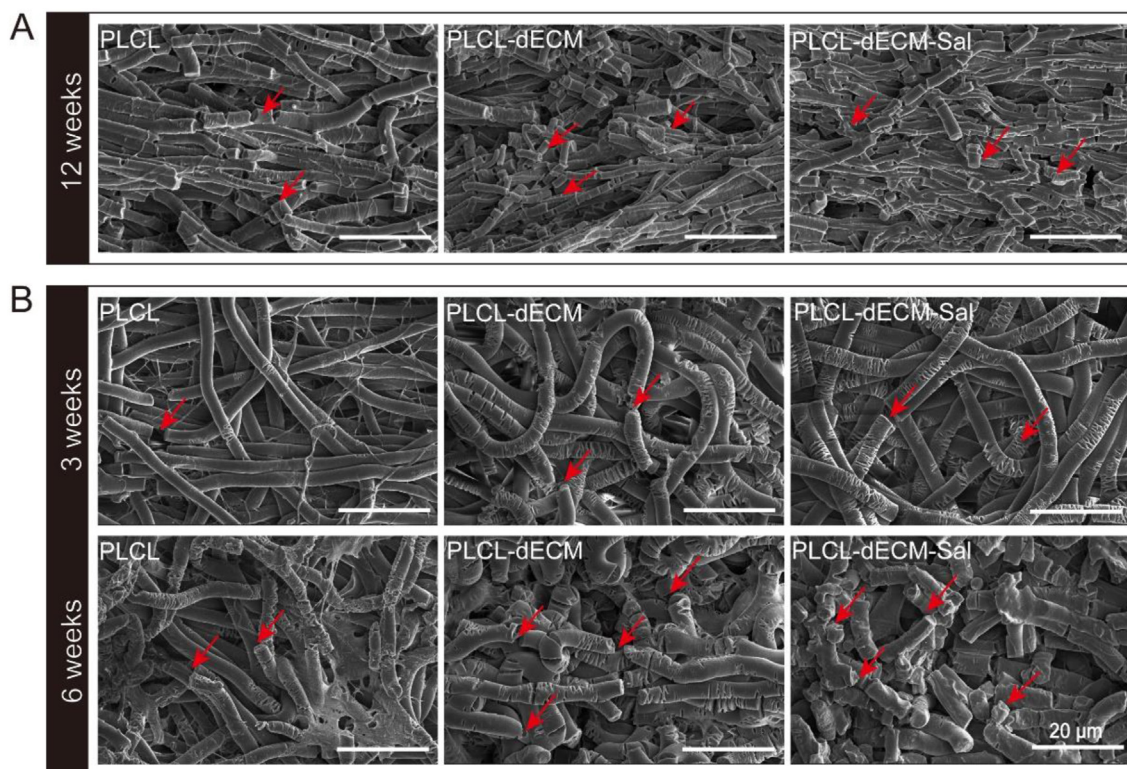

Fig. 8. Degradability of vascular grafts *in vitro* and *in vivo*. (A) Degradability of scaffolds *in vitro* 12 weeks ($n = 3$). (B) Degradation of vascular grafts *in vivo* at week 3 and week 6 ($n = 4$). (Red arrows indicated fiber fractures).

vascular calcification context remains to be determined. In future investigations, calcification may be addressed by regulating the formation of acidic environments [53], by preparing large-pore grafts to create a well-organized neointima that helps prevent calcific deposition [54], and by adding antioxidants and immunomodulatory factors into the graft to regulate the incidence of prolonged inflammatory reactions [55]. At the same time, the rat has fast blood flow and metabolism rate which could not meet well with vascular graft clinical application situation. It is necessary to do a larger and more clinical-relevant animal model to determine the effectiveness of the PLCL-dECM graft in future studies.

5. Conclusions

We developed a tri-layered biomimetic vascular graft loaded with salidroside and dECM. The grafts released salidroside from the intima layer to inhibit platelet accumulation at the blood-interface of the PLCL-dECM fibers, which prevented the occurrence of thrombus. The addition of dECM provided the advantages of rapid endothelialization and regeneration of smooth muscle layers, pivotal for achieving biofunctional SDVGs. Finally, we provide a promising method and material for the construction of SDVGs.

Author contribution

Shike Hou and Qi Lv: Conceptualization, Methodology. Yanjiao Teng: Writing – original draft. Jie Shi: Writing – review & editing. Ju He and Adam C. Midgley: Data curation. Xiaoqin Guo and Yakai Feng: Investigation. Duo Li, Xiudan Wang and Xinran Yang: Validation. Qi Lv, Jie Shi, and Shufang Wang: Funding acquisition.

Declaration of competing interest

The authors declare that they have no known competing financial interests or personal relationships that could have appeared to influence the work reported in this paper.

Data availability

Data will be made available on request.

Acknowledgements

Appendix A. Supplementary data

Supplementary data to this article can be found online at https://doi.org/10.1016/j.mtbio.2023.100709.

References

[1] S.L. Dahl, J.L. Blum, L.E. Niklason, Bioengineered vascular grafts: can we make them off-the-shelf? Trends Cardiovasc. Med. 21 (3) (2011) 83–89.

[2] D.G. Seifu, A. Purnama, K. Mequanint, D. Mantovani, Small-diameter vascular tissue engineering, Nat. Rev. Cardiol. 10 (7) (2013) 410–421.

[3] K. Wang, W. Zheng, Y. Pan, S. Ma, Y. Guan, R. Liu, M. Zhu, X. Zhou, J. Zhang, Q. Zhao, Y. Zhu, L. Wang, D. Kong, Three-layered PCL grafts promoted vascular regeneration in a rabbit carotid artery model, Macromol. Biosci. 16 (4) (2016) 608–618.

[4] M.T. Koobatian, S. Row, R.J. Smith Jr., C. Koenigsknecht, S.T. Andreadis, D.D. Swartz, Successful endothelialization and remodeling of a cell-free small-diameter arterial graft in a large animal model, Biomaterials 76 (2016) 344–358.

[5] H. Sano, M. Watanabe, T. Yamashita, K. Tanishita, R. Sudo, Control of vessel diameters mediated by flow-induced outward vascular remodeling in vitro, Biofabrication 12 (4) (2020), 045008.

[6] A. Goins, A.R. Webb, J.B. Allen, Multi-layer approaches to scaffold-based small diameter vessel engineering: a review, Mater Sci Eng C Mater Biol Appl 97 (2019) 896–912.

[7] S. Pashneh-Tala, S. MacNeil, F. Claeyssens, The tissue-engineered vascular graft-past, present, and future, Tissue Eng. B Rev. 22 (1) (2016) 68–100.

[8] P.F. Sanchez, E.M. Brey, J.C. Briceno, Endothelialization mechanisms in vascular grafts, J Tissue Eng Regen Med 12 (11) (2018) 2164–2178.

[9] S. Dimitrievska, L.E. Niklason, Historical perspective and future direction of blood vessel developments, Cold Spring Harb Perspect Med 8 (2) (2018).

[10] G. Bao, T. Jiang, H. Ravanbakhsh, A. Reyes, Z. Ma, M. Strong, H. Wang, J.M. Kinsella, J. Li, L. Mongeau, Triggered micropore-forming bioprinting of porous viscoelastic hydrogels, Mater. Horiz. 7 (9) (2020) 2336–2347.

[11] E.M. Cunnane, N.F. Davis, C.V. Cunnane, K.L. Lorentz, A.J. Ryan, J. Hess, J.S. Weinbaum, M.T. Walsh, F.J. O'Brien, D.A. Vorp, Mechanical, compositional and morphological characterisation of the human male urethra for the development of a biomimetic tissue engineered urethral scaffold, Biomaterials 269 (2021), 120651.

[12] B.R. Freedman, D.J. Mooney, Biomaterials to mimic and heal connective tissues, Adv. Mater. 31 (19) (2019), e1806695.

[13] M.B. Chan-Park, J.Y. Shen, Y. Cao, Y. Xiong, Y. Liu, S. Rayatpisheh, G.C. Kang, H.P. Greisler, Biomimetic control of vascular smooth muscle cell morphology and phenotype for functional tissue-engineered small-diameter blood vessels, J. Biomed. Mater. Res. 88 (4) (2009) 1104–1121.

[14] A. Mammoto, K. Matus, T. Mammoto, Extracellular matrix in aging aorta, Front. Cell Dev. Biol. 10 (2022), 822561.

[15] H. Cao, X. Wang, M. Chen, Y. Liu, X. Cui, J. Liang, Q. Wang, Y. Fan, X. Zhang, Childhood cartilage ECM enhances the chondrogenesis of endogenous cells and subchondral bone repair of the unidirectional collagen-dECM scaffolds in combination with microfracture, ACS Appl. Mater. Interfaces 13 (48) (2021) 57043–57057.

[16] J.A. Reid, A. Callanan, Hybrid cardiovascular sourced extracellular matrix scaffolds as possible platforms for vascular tissue engineering, J. Biomed. Mater. Res. B Appl. Biomater. 108 (3) (2020) 910–924.

[17] X. Zhang, X. Chen, H. Hong, R. Hu, J. Liu, C. Liu, Decellularized extracellular matrix scaffolds: recent trends and emerging strategies in tissue engineering, Bioact. Mater. 10 (2022) 15–31.

[18] S. Liu, L. Yao, Y. Wang, Y. Li, Y. Jia, Y. Yang, N. Li, Y. Hu, D. Kong, X. Dong, K. Wang, M. Zhu, Immunomodulatory hybrid micro-nanofiber scaffolds enhance vascular regeneration, Bioact. Mater. 21 (2023) 464–482.

[19] W. Gong, D. Lei, S. Li, P. Huang, Q. Qi, Y. Sun, Y. Zhang, Z. Wang, Z. You, X. Ye, Q. Zhao, Hybrid small-diameter vascular grafts: anti-expansion effect of electrospun poly ε-caprolactone on heparin-coated decellularized matrices, Biomaterials 76 (2016) 359–370.

[20] H. Lee, W. Kim, J. Lee, J.J. Yoo, G.H. Kim, S.J. Lee, Effect of hierarchical scaffold consisting of aligned dECM nanofibers and poly(lactide-co-glycolide) struts on the orientation and maturation of human muscle progenitor cells, ACS Appl. Mater. Interfaces 11 (43) (2019) 39449–39458.

[21] J. Shi, X. Zhang, L. Jiang, L. Zhang, Y. Dong, A.C. Midgley, D. Kong, S. Wang, Regulation of the inflammatory response by vascular grafts modified with Aspirin-Triggered Resolvin D1 promotes blood vessel regeneration, Acta Biomater. 97 (2019) 360–373.

[22] A. Stahl, D. Hao, J. Barrera, D. Henn, S. Lin, S. Moeinzadeh, S. Kim, W. Maloney, G. Gurtner, A. Wang, Y.P. Yang, A bioactive compliant vascular graft modulates macrophage polarization and maintains patency with robust vascular remodeling, Bioact. Mater. 19 (2023) 167–178.

[23] D. Liu, T. Xiang, T. Gong, T. Tian, X. Liu, S. Zhou, Bioinspired 3D multilayered shape memory scaffold with a hierarchically changeable micropatterned surface for efficient vascularization, ACS Appl. Mater. Interfaces 9 (23) (2017) 19725–19735.

[24] P. Fungaloi, R. Statius van Eps, Y.-P. Wu, J. Blankensteijn, P. Groot, H. Urk, R. Hillegersberg, G. LaMuraglia, Platelet adhesion to photodynamic therapy-treated extracellular matrix proteins, Photochem. Photobiol. 75 (4) (2007) 412–417.

[25] G. Wei, X. Xu, H. Tong, X. Wang, Y. Chen, Y. Ding, S. Zhang, W. Ju, C. Fu, Z. Li, L. Zeng, K. Xu, J. Qiao, Salidroside inhibits platelet function and thrombus formation through AKT/GSK3β signaling pathway, Aging (Albany NY) 12 (9) (2020) 8151–8166.

[26] Y. Tang, C. Vater, A. Jacobi, C. Liebers, X. Zou, M. Stiehler, Salidroside exerts angiogenic and cytoprotective effects on human bone marrow-derived endothelial progenitor cells via Akt/mTOR/p70S6K and MAPK signalling pathways, Br. J. Pharmacol. 171 (9) (2014) 2440–2456.

[27] J. Zhang, V. Kasim, Y.D. Xie, C. Huang, J. Sisjayawan, A. Dwi Ariyanti, X.S. Yan, X.Y. Wu, C.P. Liu, L. Yang, M. Miyagishi, S.R. Wu, Inhibition of PHD3 by salidroside promotes neovascularization through cell-cell communications mediated by muscle-secreted angiogenic factors, Sci. Rep. 7 (2017), 43935.

[28] Y. Xiong, Y. Wang, Y. Xiong, W. Gao, L. Teng, Salidroside alleviated hypoxia-induced liver injury by inhibiting endoplasmic reticulum stress-mediated apoptosis via IRE1alpha/JNK pathway, Biochem. Biophys. Res. Commun. 529 (2) (2020) 335–340.

[29] W.L. Pu, M.Y. Zhang, R.Y. Bai, L.K. Sun, W.H. Li, Y.L. Yu, Y. Zhang, L. Song, Z.X. Wang, Y.F. Peng, H. Shi, K. Zhou, T.X. Li, Anti-inflammatory effects of Rhodiola rosea L.: a review, Biomed. Pharmacother. 121 (2020), 109552.

[30] H. Kuang, Y. Wang, Y. Shi, W. Yao, X. He, X. Liu, X. Mo, S. Lu, P. Zhang, Construction and performance evaluation of Hep/silk-PLCL composite nanofiber small-caliber artificial blood vessel graft, Biomaterials 259 (2020), 120288.

[31] J.L. Francis, J.B. Groce 3rd, Challenges in variation and responsiveness of unfractionated heparin, Pharmacotherapy 24 (8) (2004) 108–119.

[32] X. Yuan, W. Li, B. Yao, Z. Li, D. Kong, S. Huang, M. Zhu, Tri-layered vascular grafts guide vascular cells' native-like arrangement, Polymers 14 (7) (2022).

[33] D. Zhi, Q. Cheng, A.C. Midgley, Q. Zhang, T. Wei, Y. Li, T. Wang, T. Ma, M. Rafique, S. Xia, Y. Cao, Y. Li, J. Li, Y. Che, M. Zhu, K. Wang, D. Kong, Mechanically reinforced biotubes for arterial replacement and arteriovenous grafting inspired by architectural engineering, Sci. Adv. 8(11) eabl3888.

[34] K. Wang, Q. Zhang, L. Zhao, Y. Pan, T. Wang, D. Zhi, S. Ma, P. Zhang, T. Zhao, S. Zhang, W. Li, M. Zhu, Y. Zhu, J. Zhang, M. Qiao, D. Kong, Functional modification of electrospun poly(epsilon-caprolactone) vascular grafts with the fusion protein VEGF-HGFI enhanced vascular regeneration, ACS Appl. Mater. Interfaces 9 (13) (2017) 11415–11427.

[35] G. Pula, U. Mayr, C. Evans, M. Prokopi, D.S. Vara, X. Yin, Z. Astroulakis, Q. Xiao, J. Hill, Q. Xu, M. Mayr, Proteomics identifies thymidine phosphorylase as a key regulator of the angiogenic potential of colony-forming units and endothelial progenitor cell cultures, Circ. Res. 104 (1) (2009) 32–40.

[36] K.L. DeCicco-Skinner, G.H. Henry, C. Cataisson, T. Tabib, J.C. Gwilliam, N.J. Watson, E.M. Bullwinkle, L. Falkenburg, R.C. O'Neill, A. Morin, J.S. Wiest, Endothelial cell tube formation assay for the in vitro study of angiogenesis, J. Vis. Exp. 91 (2014), e51312.

[37] M. Zhu, Y. Wu, W. Li, X. Dong, H. Chang, K. Wang, P. Wu, J. Zhang, G. Fan, L. Wang, J. Liu, H. Wang, D. Kong, Biodegradable and elastomeric vascular grafts enable vascular remodeling, Biomaterials 183 (2018) 306–318.

[38] P.M. Crapo, T.W. Gilbert, S.F. Badylak, An overview of tissue and whole organ decellularization processes, Biomaterials 32 (12) (2011) 3233–3243.

[39] S. Nagata, R. Hanayama, K. Kawane, Autoimmunity and the clearance of dead cells, Cell 140 (5) (2010) 619–630.

[40] A. Hasan, A. Memic, N. Annabi, M. Hossain, A. Paul, M.R. Dokmeci, F. Dehghani, A. Khademhosseini, Electrospun scaffolds for tissue engineering of vascular grafts, Acta Biomater. 10 (1) (2014) 11–25.

[41] A.F. Pellegata, M.A. Asnaghi, I. Stefani, A. Maestroni, S. Maestroni, T. Dominioni, S. Zonta, G. Zerbini, S. Mantero, Detergent-enzymatic decellularization of swine blood vessels: insight on mechanical properties for vascular tissue engineering, BioMed Res. Int. 2013 (2013), 918753.

[42] C. Zhang, R. Cha, C. Wang, X. Chen, Z. Li, Q. Xie, L. Jia, Y. Sun, Z. Hu, L. Zhang, F. Zhou, Y. Zhang, X. Jiang, Red blood cell membrane-functionalized Nanofibrous tubes for small-diameter vascular grafts, Biomaterials 297 (2023), 122124.

[43] Y. Ge, Q. Wang, X. Qin, S. Li, Z. Liu, Y. Lin, X. Li, X. Cai, Tetrahedral framework nucleic acids connected with MicroRNA-126 mimics for applications in vascular inflammation, remodeling, and homeostasis, ACS Appl. Mater. Interfaces 14 (17) (2022) 19091–19103.

[44] S.W. Cho, J.E. Lim, H.S. Chu, H.J. Hyun, C.Y. Choi, K.C. Hwang, K.J. Yoo, D.I. Kim, B.S. Kim, Enhancement of in vivo endothelialization of tissue-engineered vascular grafts by granulocyte colony-stimulating factor, J. Biomed. Mater. Res. 76 (2) (2006) 252–263.

[45] J.S. Lee, K. Lee, S.H. Moon, H.M. Chung, J.H. Lee, S.H. Um, D.I. Kim, S.W. Cho, Mussel-inspired cell-adhesion peptide modification for enhanced endothelialization of decellularized blood vessels, Macromol. Biosci. 14 (8) (2014) 1181–1189.

[46] X. Zhang, Y. Wang, J. Liu, J. Shi, D. Mao, A.C. Midgley, X. Leng, D. Kong, Z. Wang, B. Liu, S. Wang, A metal-organic-framework incorporated vascular graft for sustained nitric oxide generation and long-term vascular patency, Chem. Eng. J. 421 (2021).

[47] C.K. Hashi, Y. Zhu, G.-Y. Yang, W.L. Young, B.S. Hsiao, K. Wang, B. Chu, S. Li, Antithrombogenic property of bone marrow mesenchymal stem cells in nanofibrous vascular grafts, Proc. Natl. Acad. Sci. USA 104 (29) (2007) 11915–11920.

[48] A. Ranella, M. Barberoglou, S. Bakogianni, C. Fotakis, E. Stratakis, Tuning cell adhesion by controlling the roughness and wettability of 3D micro/nano silicon structures, Acta Biomater. 6 (7) (2010) 2711–2720.

[49] Q. Zhao, H. Cui, J. Wang, H. Chen, Y. Wang, L. Zhang, X. Du, M. Wang, Regulation effects of biomimetic hybrid scaffolds on vascular endothelium remodeling, ACS Appl. Mater. Interfaces 10 (28) (2018) 23583–23594.

[50] W. Li, P. Wu, Y. Zhang, A.C. Midgley, X. Yuan, Y. Wu, L. Wang, Z. Wang, M. Zhu, D. Kong, Bilayered polymeric micro- and nanofiber vascular grafts as abdominal aorta replacements: long-term in vivo studies in a rat model, ACS Appl. Bio Mater. 2 (10) (2019) 4493–4502.

[51] M. Fakhry, M. Roszkowska, A. Briolay, C. Bougault, A. Guignandon, J.I. Diaz-Hernandez, M. Diaz-Hernandez, S. Pikula, R. Buchet, E. Hamade, B. Badran, L. Bessueille, D. Magne, TNAP stimulates vascular smooth muscle cell trans-differentiation into chondrocytes through calcium deposition and BMP-2 activation: possible implication in atherosclerotic plaque stability, Biochim. Biophys. Acta, Mol. Basis Dis. 1863 (3) (2017) 643–653.

[52] X. Zhuang, A. Maimaitijiang, Y. Li, H. Shi, X. Jiang, Salidroside inhibits high-glucose induced proliferation of vascular smooth muscle cells via inhibiting mitochondrial fission and oxidative stress, Exp. Ther. Med. 14 (1) (2017) 515–524.

[53] N. Reiter, L. El-Shabrawi, B. Leinweber, A. Berghold, E. Aberer, Calcinosis cutis: part I. Diagnostic pathway, J. Am. Acad. Dermatol. 65 (1) (2011) 1–12, quiz 13-14.

[54] S. Tara, H. Kurobe, K.A. Rocco, M.W. Maxfield, C.A. Best, T. Yi, Y. Naito, C.K. Breuer, T. Shinoka, Well-organized neointima of large-pore poly(L-lactic acid) vascular graft coated with poly(L-lactic-co-epsilon-caprolactone) prevents calcific deposition compared to small-pore electrospun poly(L-lactic acid) graft in a mouse aortic implantation model, Atherosclerosis 237 (2) (2014) 684–691.

[55] B. Jiang, R. Suen, J.J. Wang, Z.J. Zhang, J.A. Wertheim, G.A. Ameer, Vascular scaffolds with enhanced antioxidant activity inhibit graft calcification, Biomaterials 144 (2017) 166–175.